# A New Monthly Climatology of Global Radiation for the Arctic and Comparisons with NCEP–NCAR Reanalysis and ISCCP-C2 Fields

MARK C. SERREZE

*Cooperative Institute for Research in Environmental Sciences, University of Colorado, Boulder, Colorado*

JEFFREY R. KEY

*Department of Geography, Boston University, Boston, Massachusetts*

JASON E. BOX, JAMES A. MASLANIK, AND KONRAD STEFFEN

*Cooperative Institute for Research in Environmental Sciences, University of Colorado, Boulder, Colorado*

(Manuscript received 3 February 1997, in final form 3 June 1997)

ABSTRACT

Measurements from the Russian ''North Pole'' series of drifting stations, the United States drifting stations ''T-3'' and ''Arlis II,'' land stations, and, where necessary, over the northern North Atlantic and coastal Greenland, empirically derived values from earlier Russian studies are used to compile a new gridded monthly climatology of global (downwelling shortwave) radiation for the region north of 65°N. Spatio-temporal patterns of fluxes and effective cloud transmittance are examined and comparisons are made with fields from the National Centers for Environmental Prediction–National Center for Atmospheric Research (NCEP–NCAR) reanalysis and those derived from the International Satellite Cloud Climatology Project (ISCCP) C2 (monthly) cloud product.

All months examined (March–October) show peak fluxes over the Greenland ice sheet. March, September, and October feature a strong zonal component. Other months exhibit an asymmetric pattern related to cloud fraction and optical depth, manifested by an Atlantic side flux minimum. For June, the month of maximum insolation, fluxes increase from less than 200 W $m^{-2}$ in the Norwegian and Barents seas to more than 300 W $m^{-2}$ over the Pacific side of central Arctic Ocean extending into the Beaufort Sea. June fluxes of more than 340 W $m^{-2}$ are found over the Greenland ice sheet. Effective cloud transmittance, taken as the ratio of the observed flux to the modeled clear sky flux, is examined for April–September. Values for the Atlantic sector range from 0.50–0.60, contrasting with the central Arctic Ocean where values peak in April at 0.75–0.80, falling to 0.60–0.65 during late summer and early autumn. A relative Beaufort Sea maximum is well expressed during June. The NCEP–NCAR and ISCCP products capture 50%–60% of the observed spatial variance in global radiation during most months. However, the NCEP–NCAR fluxes are consistently high, with Arctic Ocean errors in excess of 60 W $m^{-2}$ during summer, reflecting problems in modeled cloud cover. ISCCP fluxes compare better in terms of magnitude.

## 1. Introduction

Largely due to feedbacks involving the surface energy budget, the Arctic is considered to be a region of particular importance and vulnerability to global climate change (IPCC 1990). Although many potential feedback processes have been identified (Curry et al. 1996), the best known is the ice-albedo feedback, in which an initial temperature change may be amplified through attendant changes in terrestrial snow cover, snow on sea ice, and sea-ice extent. Although the importance of feedback mechanisms is recognized from modeling experiments, there is a need for improved datasets of surface energy budget components for process studies, the development of single-column process models, and model validation. Detailed measurement programs planned for the (1997–98) Surface Heat Budget of the Arctic Ocean (SHEBA) field experiment in the Beaufort Sea should help to fulfill some of these needs, but existing data sources also need to be assembled to provide basic climatologies.

The often-cited Arctic radiation climatologies by Marshunova (1961), Marshunova and Chernigovskii (1966, 1971), Vowinckel and Orvig (1962, 1963, 1964), and Gavrilova (1963) are based on data from coastal sites and sparse Arctic Ocean data then available from the Russian ''North Pole'' (NP) series of drifting ice stations. Fletcher (1966) noted that differences between

*Corresponding author address:* Dr. Mark C. Serreze, Cooperative Institute for Research in Environmental Science, University of Colorado, Campus Box 449, Boulder, CO 80309-0449.
E-mail: serreze@kryos.colorado.edu

© 1998 American Meteorological Society

Marshunova's and Vowinckel and Orvig's climatologies are much greater than the estimated accuracies. On this basis, he questioned Gavrilova's (1963) arguments that global radiation in the Arctic is known to an accuracy of 2.5% for annual fluxes, 5%–10% for monthly fluxes, 10%–15% for absorbed solar radiation, 15%–20% for outgoing longwave radiation, and 20%–30% for the radiation balance. Nevertheless, he concluded that the work of Marshunova (1961) probably represented the most accurate description of the Arctic radiation climate. Ohmura (1981) arrived at the same conclusion 15 yr later. Much more recently, Marshunova and Mishin (1994) summarized results from the NP stations 2–31, covering the period 1950–91.

The World Climate Research Program (WMO 1992) has identified the need to develop and validate satellite-derived surface radiation datasets. Reviews of techniques to infer surface fluxes from top of the atmosphere radiances and problems in application to high latitudes are provided by Schmetz (1989) and Raschke et al. (1992). Errors in satellite-derived solar fluxes for lower latitudes are near 5% for monthly sums, 9% for daily sums, and 5%–50% for hourly sums (Schmetz 1989). An example of an Arctic application is given by Schweiger and Key (1994), where surface and top of the atmosphere radiative fluxes were computed using the monthly cloud product (C2) of the International Satellite Cloud Climatology Project (ISCCP) (cf. Rossow and Zhang 1995) for the period 1984–90. Although the ISCCP-C2 cloud amount is generally underestimated, especially during summer, spatially averaged shortwave fluxes were found to agree well with the climatology of Marshunova (1961), in part due to balancing overestimates of cloud optical depth. By comparison, downwelling longwave fluxes were found to be too low, apparently in part due to underestimates of low cloud cover.

From the perspective of climate change detection and modeling, the estimated potential error in surface net radiative fluxes of 11–20 W $m^{-2}$ is too large. Estimates of the net radiative warming effect due to a doubling of $CO_2$ are on the order of 4–11 W $m^{-2}$. Given the uncertainty in satellite-derived fluxes, the relatively short satellite record, and the fact that more than 30 yr of surface data have been collected at Arctic land and drifting ice stations, new climatologies of surface radiative fluxes are needed (cf. Marshunova and Mishin 1994). We have initiated efforts to provide improved climatologies of the Arctic surface radiation budget, starting with global radiation. This new climatology is based primarily on records from the NP series of drifting stations, U.S. drifting stations, and land stations. Estimated values from Marshunova and Chernigovskii (1971) and Smetannikovoi (1983) are used for locations along coastal Greenland and the North Atlantic where actual observations are scanty or nonexistent (Fig. 1).

Here we describe the assembly of this dataset and discuss spatio-temporal patterns of insolation and effective cloud transmittance. Comparisons are made with radiation fields being provided by the National Centers for Environmental Prediction–National Center for Atmospheric Research (NCEP–NCAR) reanalysis effort (Kalnay et al. 1996), representing part of an ongoing effort to assess the veracity of the model outputs for studies of Arctic climate variability. Comparisons are also made with fields computed using the ISCCP-C2 cloud climatology (Schweiger and Key 1994). Work is under way to provide a new radiation climatology using the ISCCP ''D'' product, now in production, which promises improved retrieval of Arctic cloud properties. However, more robust validations of the existing ISCCP climatology are needed to assess whether expected improvements in the D products are significant.

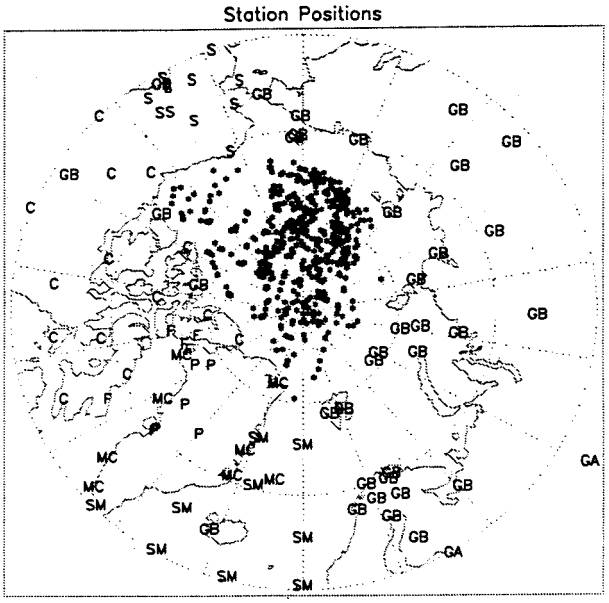


FIG. 1. Location map of the Arctic showing the distribution of data used in the study and their sources: GEBA (GB); Canadian Atmospheric Environment Service (C); SAMSON (S); PARCA (P); Gavrilova (GA); field experiments (F); Russian and U.S. drifting stations (*); Marshunova and Chernigovskii (MC); Smetannikovoi (SM). The latter two sources provide only estimated values (see text). The drifting station locations are plotted at the average monthly positions; some plotted positions represent data for multiple months.

## 2. Datasets

### *a. Drifting stations*

Starting in 1950, the Soviets maintained two and sometimes three North Pole drifting ice stations in the Arctic Ocean. Thirty ice stations were manned between 1950 and 1991 (NP-2 through NP-31; NP-1, the first ice station, operated during 1937–38). Along with other synoptic meteorological and scientific observations, radiation measurements were made on a regular basis. The average duration of each station was 2.4 yr. Russian scientists at the Arctic and Antarctic Research Institute

have assembled these records to provide monthly averages at the mean positions of the stations, climatological monthly fluxes on a coarse lat–long grid, and daily values from NP-17 through NP-31 (Marshunova and Mishin 1994). These data were obtained from a CD-ROM compiled by the University of Washington's Polar Science Center (PSC) and the University of Colorado's National Snow and Ice Data Center (NSIDC).

Radiation measurements from the U.S. ice island ''T-3'' (also known as Fletcher's Ice Island and Ice Station B) for primarily spring–autumn months of 1953, 1957–59, and 1971–73 were digitized from tables in Marshunova and Chernigovskii (1971) and the technical report of Weller and Holmgren (1974), with positions obtained from the PSC and the latter report. From 1953–59, T-3 drifted from north of Ellesmere Island along the Canadian coast and into the Beaufort Sea. It then continued to drift clockwise around the Canada Basin again to north of Ellesmere Island, remaining nearly motionless at approximately 85°N, 85°W during 1971–73.

Monthly radiation means and positions from U.S. ''Arlis II'' for January 1964–May 1965 were digitized from tables published by Roulet (1969). During this interval, Arlis II drifted from near the Pole to just north of Greenland. Efforts were also made to recover radiation fluxes in the Beaufort Sea collected at four drifting camps during the Arctic Ice Dynamics Joint Experiment (AIDJEX) (Pautzke and Hornof 1978). Careful inspection of these data revealed numerous large errors. Following recommendations from a scientist involved in the measurement program (G. Weller 1997, personal communication), these data were discarded.

The resulting number of available station months from combining the Russian NP and U.S. drifting records is over 70 from June through September and over 40 from March through May as well as October. Few data points are available from November through February, ranging from one in December to 15 in February.

### *b. Land stations*

Data from land stations were obtained from several sources. The Global Energy Balance Archive (GEBA; Ohmura and Gilgen 1991) contains monthly means of global radiation from 57 land stations north of 60°N. Records range in length from 1 to 49 yr, with data for stations in continual operation available through 1987. We also use monthly data from nine Alaska stations from the National Oceanic and Atmospheric Administration (NOAA) Solar and Meteorological Surface Observations (SAMSON) archive north of 60°N for the time period 1961–90. Monthly records of at least 20 yr duration for 14 sites in the Canadian Arctic, obtained from the Atmospheric Environment Service, Ottawa, and climatological monthly means for two Eurasian sites from Gavrilova (1963) are also included in our analysis.

Several years of monthly data (1971–73) were obtained for Broughton Island, off the east coast of Baffin Island, collected as part of a field experiment (Jacobs et al. 1974) and for the Carey Islands (1973–74), Coburg Island (1972–74), and Cape Herschel (1973–74), collected during the Baffin Bay ''North Water Experiment'' (Muller et al. 1976). Lastly, monthly data were obtained for six sites over the Greenland Ice Sheet from the Program for Arctic Regional Climate Assessment (PARCA) (headed by K. Steffen, University of Colorado, and sponsored by the National Aeronautics and Space Administration and the National Science Foundation). Four sites over western Greenland provide a single year of data between 1995 and 1996, with the summit station providing only summer data for 1996. A longer record, complete for 1994–95 with partial records for 1990–93 and 1996, is provided from the PARCA University of Colorado Greenland Camp.

### *c. North Atlantic sector and coastal Greenland*

It was found that the above archives provide poor coverage of the North Atlantic between about 60° and 65°N and for coastal Greenland. To obtain coverage over these areas, it was necessary to resort to calculated rather than measured values. For coastal Greenland stations and Jan Mayen, we made use of values from Marshunova and Chernigovskii (1971). For the North Atlantic, a series of points was chosen from contour maps provided by Smetannikovoi (1983). Marshunova and Chernigovskii (1971) employ the method of Vowinkel and Orvig (1964) to estimate station fluxes from consideration of clear-sky radiation and attenuation by aerosols, cloud amount, and type. These relationships are then assumed to hold for other stations for which no fluxes are measured. The Smetannikovoi (1983) values are calculated similarly. Marshunova and Chernigovskii (1971) find that this technique is generally accurate within 10%, but their Table 13 indicates that it may be in error by as much as 25% in autumn. Key et al. (1996) compare a variety of downwelling shortwave flux parameterizations, similar to those of Marshunova and Chernigovskii (1971) and Smetannikovoi (1983), to surface measurements. Their results agree with the findings of Marshunova and Chernigovskii (1971).

## 3. Data processing

### *a. Interpolation*

Our objective is to provide long-term monthly means at a regular grid of points. A Cressman interpolation (Cressman 1959) was used to interpolate the irregularly spaced data to a 100 × 100-km grid on the north polar Lambert equal-area projection known as the NSIDC EASE-grid (Armstrong and Brodzik 1995). This is a lower-resolution form of the same equal-area projection being used at NSIDC for producing Special Sensor Microwave Imager (SSM/I) global brightness temperature grids and geophysical products from the NOAA/NASA

SSM/I Pathfinder program. The Cressman interpolation has the form

$$F_{ease} = \sum F_i W_i / \sum W_i$$
$$W_i = (N^2 - d^2)/(N^2 + d^2),$$

where $F_{ease}$ is the flux at a desired EASE-grid point, $F_i$ is the flux at an observed location $i$, $W_i$ is the weight given to that observation, $d$ is the distance between the observation and the EASE-grid point, and $N$ is the search radius, beyond which the weight is zero. An initial search radius is set, with the summations performed for all observations falling within that radius. If no observation falls within that radius, the search is extended over larger values of $N$.

The use of the raw values in the interpolation procedure may introduce biases related to latitudinal dependencies of the flux. Therefore, the interpolation is instead based on values expressed as the difference between the observed radiation ($G_{obs}$) and an estimate of the clear-sky downwelling shortwave flux ($G_{clr}$). The adjustment by $G_{clr}$ essentially normalizes the data with respect to latitudinal variations in solar zenith angle/day length and associated path-length dependencies of noncloud atmospheric absorption and scattering. It also acts to normalize the data with respect to the minor effect of varying surface albedo ($G_{clr}$ tends to increase with respect to albedo due to the effects of multiple scattering). After the interpolation, $G_{clr}$ is added back to the gridpoint values.

The $G_{clr}$ is computed using a neural network implementation of the two-stream radiative transfer model used by Schweiger and Key (1994) that was employed in the computation of radiative fluxes from the ISCCP-C2 cloud data (see Key et al. 1997 for details). The clear-sky flux calculations were done using ISCCP-C2 all-sky surface albedos (Schweiger et al. 1993), an aerosol optical depth of 0.05 representing background tropospheric conditions, month-specific total precipitable water ranging from 2000 g m$^{-2}$ (January) to 20 000 g m$^{-2}$ (July) (see Serreze et al. 1995), and total column ozone of 7 g m$^{-2}$ (327 Dobson units). The effect of uncertainties in these quantities is small; for example, for a 20% error in an albedo of 0.85, the error in a calculated flux of 400 W m$^{-2}$ is only 5 W m$^{-2}$.

The land data sources with monthly resolution vary widely in terms of record length, with some of the land and ocean data records expressed instead as climatological monthly means. With few exceptions, each individual monthly drifting station record represents a sample from a unique location. Simply passing all available data values into the interpolation without addressing these inconsistencies would result in serious spatial biases. Similar to the procedure used by Serreze et al. (1995) to provide a gridded Arctic climatology of precipitable water and vertically integrated water vapor fluxes, we adopted a two-step interpolation approach whereby the drifting station and fixed-location records are equally represented.

First, we passed all individual monthly values from the drifting stations into the interpolation (each adjusted by the climatological clear-sky flux), providing climatological monthly means at ocean grid points only (determined from a land–ocean mask). We required that for each grid point, the interpolated value be based on data from at least five different years; otherwise, it was coded as missing. We initially used a 500-km search radius. If fewer than five values were represented in the interpolated flux, the search radius was enlarged to 750 km.

The monthly land station measurements were then processed to provide climatological monthly means, also expressed as departures from clear-sky values. Climatological means based on fewer than 3 yr were discarded. The exception is for the Greenland Ice Sheet stations. Means for all of these irregularly distributed fixed locations were then appended to the calculated values described in section 2c and ocean gridpoint means derived from the initial interpolation, with the combined dataset then passed through a second interpolation, using search radii of 500, 750, 1000, and 1250 km and a minimum of two values for each radius. The larger search radius was necessary due to the comparatively sparse distribution of the land stations. Initial results indicated a regional problem related to sharp flux gradients between the PARCA Greenland Ice Sheet stations and surrounding coastal sites. Consequently, we modified the interpolation so that fluxes over central Greenland are interpolated from the PARCA values only.

As a result of the second interpolation, ocean grid points experience some additional adjustment by surrounding ocean points or, if near the coast, from land stations. In turn, coastal land grid points will be adjusted by the ocean grid values. Few observations are available for the drifting stations from November through February, resulting in missing data values over the central Arctic Ocean. Corresponding values of $G_{clr,}$ are, of course, very small, generally less than 15 W m$^{-2}$ during this time of year. Although we limit discussion in this paper to March–October, for the sake of completeness we simply filled missing values for which $G_{clr}$ is less than 15 W m$^{-2}$ by multiplying $G_{clr}$ by an assumed effective cloud transmittance of 0.60 (see section 4c). Our two-step interpolation and the latter adjustment provided nearly complete coverage for all EASE-grid points north of 65°N. As such, we also restrict discussion of results to this area.

### *b. Limitations*

We are well aware of limitations in our climatology. Regarding the raw data themselves, the absolute accuracy of the radiometers used for the measurements is generally ±5–10 W m$^{-2}$. However, the actual accuracy

may be less than that stated if the sensors were calibrated under conditions unlike those in the Arctic, for example, differences in the direct/diffuse ratio over high albedo surfaces and in the spectral distribution of solar radiation due to lower water vapor amounts. Sensor drift is assumed to be negligible under the assumption that the sensors underwent regular evaluation, maintenance, and replacement when necessary. The datasets described above have been quality controlled by the investigators who developed them. As such, we use these data largely as provided. Obvious outliers were flagged through manual inspection and limits checks. However, when the solar zenith angle is extreme (e.g., greater than 85°), measurement errors can be large due to limitations in the cosine response of the instruments and multiple reflections within the radiometer domes.

A two-stream model was used to train the neural network used for the computation of $G_{clr}$ [Streamer; see Key (1997) for details]. The same two-stream model was used by Schweiger and Key (1994) to compute surface radiative fluxes from the ISCCP C2 cloud data product. Unfortunately, the accuracy of a two-stream model decreases with increasing solar zenith angle (cf. Toon et al. 1989), particularly under cloudy conditions. For clear-sky conditions the error tends to be small. Comparisons with a discrete-ordinate model [DISORT (Stamnes et al. 1988) in Streamer], using 24 streams, solar zenith angles from 40°–80°, an aerosol optical depth of 0.1, and a visible surface albedo of 0.7, indicate that the two-stream model overestimates the downwelling shortwave flux by less than 1%. For cloudy conditions, the two-stream model overestimates the flux by up to 10% for overcast conditions with a liquid water cloud optical depth of 10 and other conditions as in the clear case. Additionally, the neural network used to estimate $G_{clr}$ has only been trained up to solar zenith angles of 85°. These zenith angle problems are primarily limited to the months October–March when fluxes are small, especially at high latitudes. As noted above, missing values for which $G_{clr}$ is less than 15 W m$^{-2}$ were filled using an assumed effective cloud transmittance 0.60.

Regarding the interpolations, we acknowledge that as our gridded dataset is a composite of many sources covering different areas and from different time periods, spatial variation will to some extent be influenced by temporal sampling. Although, on a year-to-year basis, the drifting stations provide only one or two points per month, taken over the entire period of record they provide reasonably good coverage (Fig. 1). The coverage is fairly sparse over the Canadian and Eurasian sectors, but apart from the short records for the Northwater region and Broughton Island, the station means are based on many years (a 23-yr modal station duration for the GEBA records). Clearly we would like to have data for more years over Greenland, but we are limited by the record presently available. Results for the northern North Atlantic and coastal Greenland, which are based largely on empirically derived values, should also be viewed cautiously. Because the interpolations are based on a large search radius, inhomogeneities in the gridded fields due to data sampling problems will tend to be minimized. However, by the same token, real local variations are smoothed.

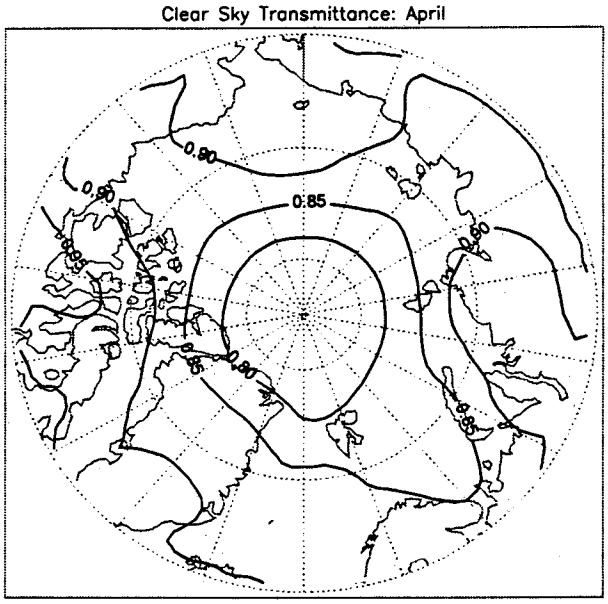


FIG. 2. Calculated clear-sky transmittance for Apr.

## 4. Results

### *a. Factors controlling global radiation*

The primary control on the global radiation flux reaching the surface is the zonally symmetric distribution of the top of atmosphere (TOA) or extraterrestrial flux. At the North Pole, the TOA flux is zero from the autumnal to spring equinoxes. By contrast, although the solar zenith angle at local noon at the summer solstice is still a large 66.5°, the attendant 24-h daylight yields a daily mean TOA flux of 522 W m$^{-2}$, as compared to only 383 W m$^{-2}$ at the equator. Because of the combined effects of day length and solar zenith angle, the monthly mean TOA flux for northern high latitudes increases with latitude from May–August, decreasing with latitude in other months. However, the maximum flux that can be received at the surface is $G_{clr}$, which, unlike the TOA flux, includes the effects of atmospheric path length and, to a minor extent, surface albedo (see section 3a). Figure 2 shows the field of estimated clear-sky transmittance, taken as the ratio between our modeled $G_{clr}$ and TOA fluxes (the latter also taken from ISCCP-derived fields) for April. The clear-sky transmittance is lower at high latitudes because of the longer path length, such that the latitudinal gradient in $G_{clr}$ is sharper than for the TOA flux. As path length decreases with elevation, other factors being equal, fluxes will be higher over high-elevation surfaces such as the Greenland ice sheet.

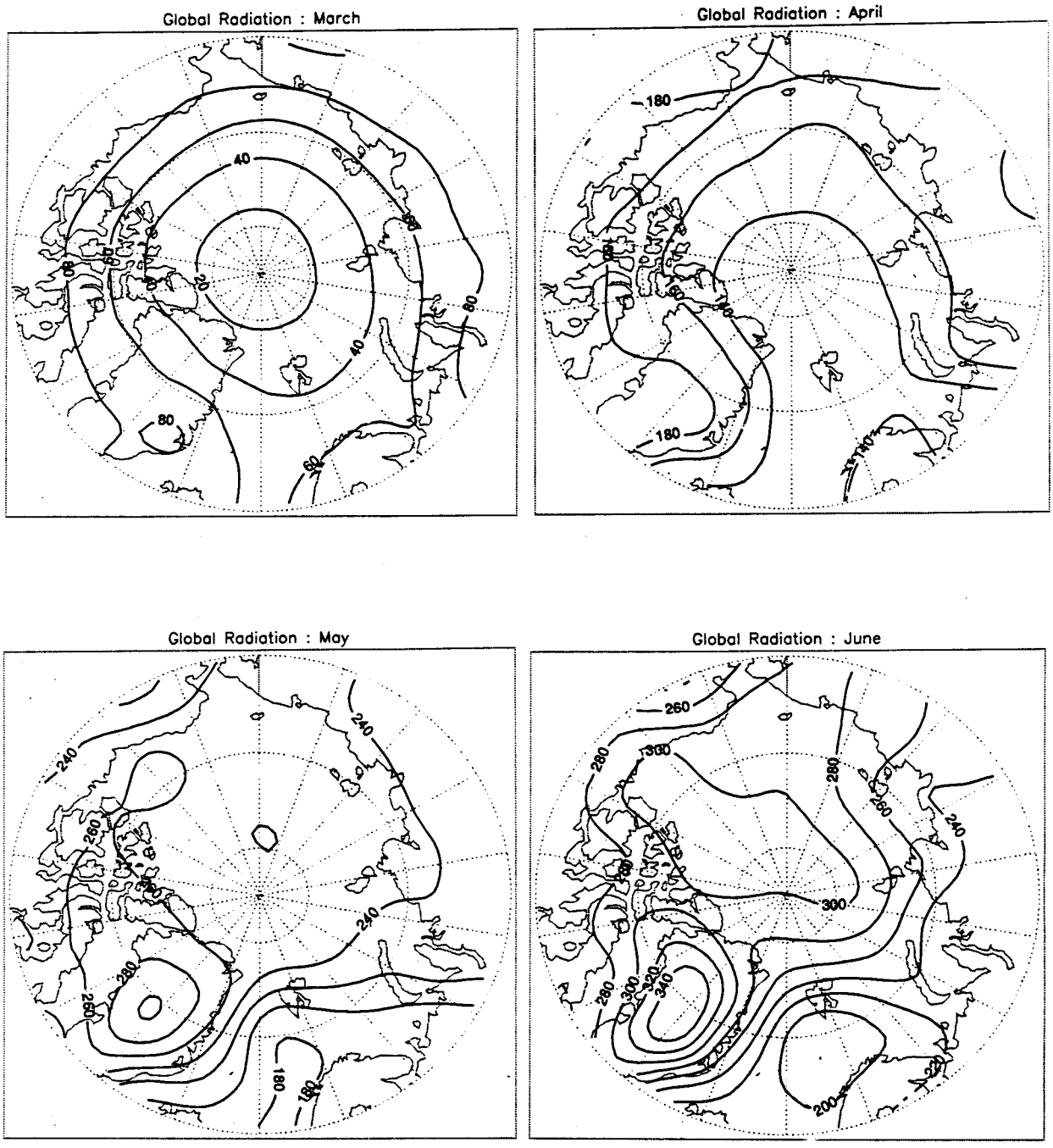


FIG. 3. Observed monthly average global radiation fluxes for Mar–Oct (W m$^{-2}$).

Clouds generally reduce the downwelling shortwave flux at the surface due to their high reflectivity (60%–75% for Arctic stratus) (Herman 1977) and, to a lesser extent, cloud absorption (Herman and Curry 1984). However, cloud attenuation is partially offset for high albedo surfaces due to multiple reflections between the surface and the cloud (Wendler et al. 1981; Shine 1984). In fact, the proportion of the downwelling shortwave flux resulting from multiple reflections can be significant and must be considered along with scattering, absorption, and transmission through the atmosphere.

A summary of surface-based climatologies for the Arctic (Huschke 1969; Warren et al. 1986, 1988) indicates that the total cloud fraction during the winter half of the year ranges from 40% to 70% but with uncertainty during months of polar darkness (Hahn et al. 1995). The greatest cloud amounts are found over the Atlantic side of the Arctic Ocean where storm activity

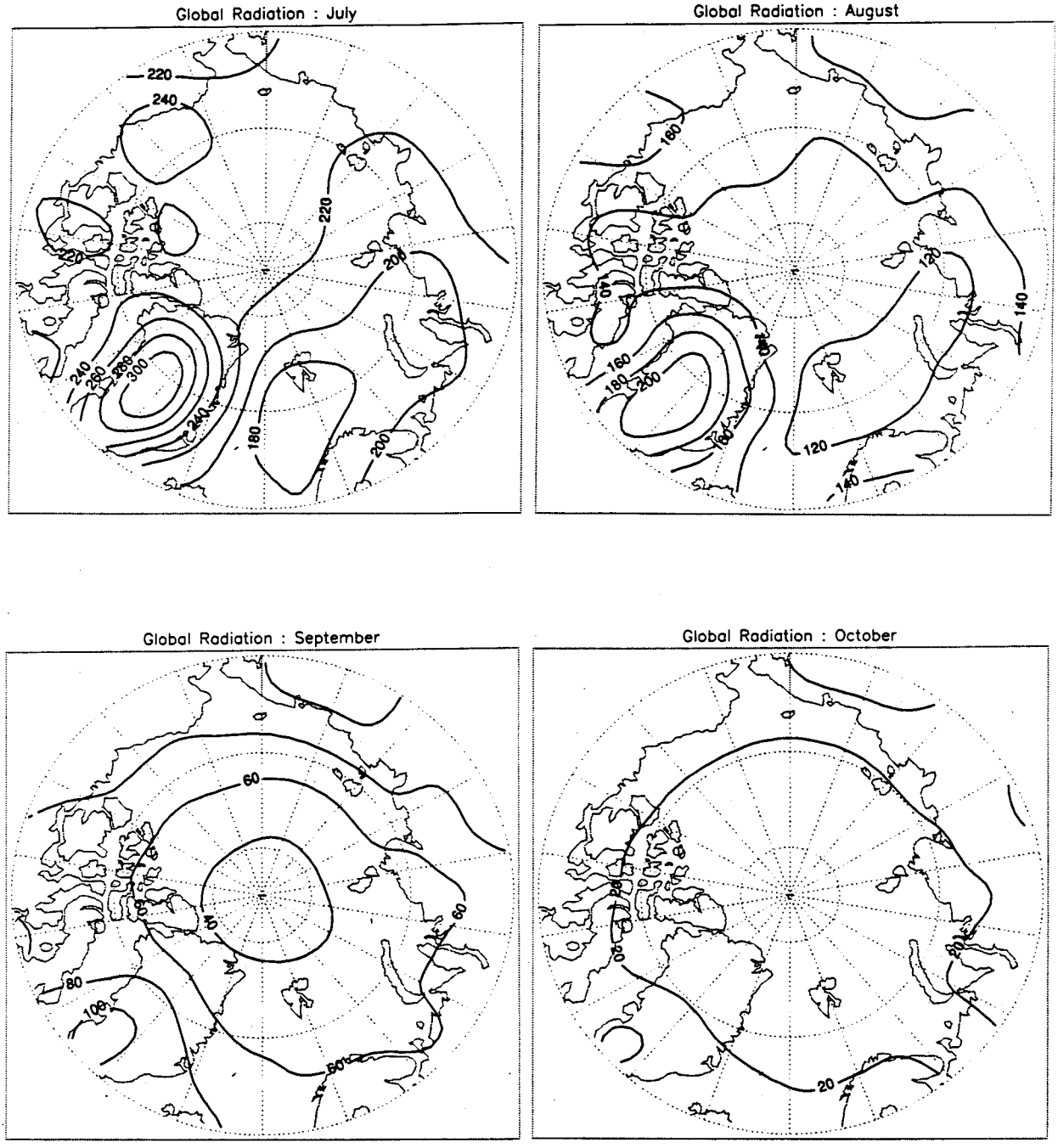


FIG. 3. (*Continued*)

associated with the primary North Atlantic cyclone track is frequent and water vapor is relatively abundant (Serreze et al. 1993). Cloud cover is typically more limited over land, the sea-ice cover, and over the central Arctic Ocean in particular, where water vapor is less abundant, the boundary layer is more stable, and anticyclonic conditions are common (Shine et al. 1984; Serreze et al. 1993). Total cloud fractions rise to between 70% and 90% in summer with a rapid increase between May and June, characterized by extensive low-level, optically thin stratus over the ocean. Although summer cloud cover is more evenly distributed, cloudiness over the Beaufort Sea region remains relatively limited, as mean anticyclonic conditions typically prevail during June and July. This Beaufort Sea cloud minimum is evident in the regional analysis by Serreze and Rehder (1990) for June, the July results from the combined Warren et al. (1986, 1988) land and ocean climatologies examined

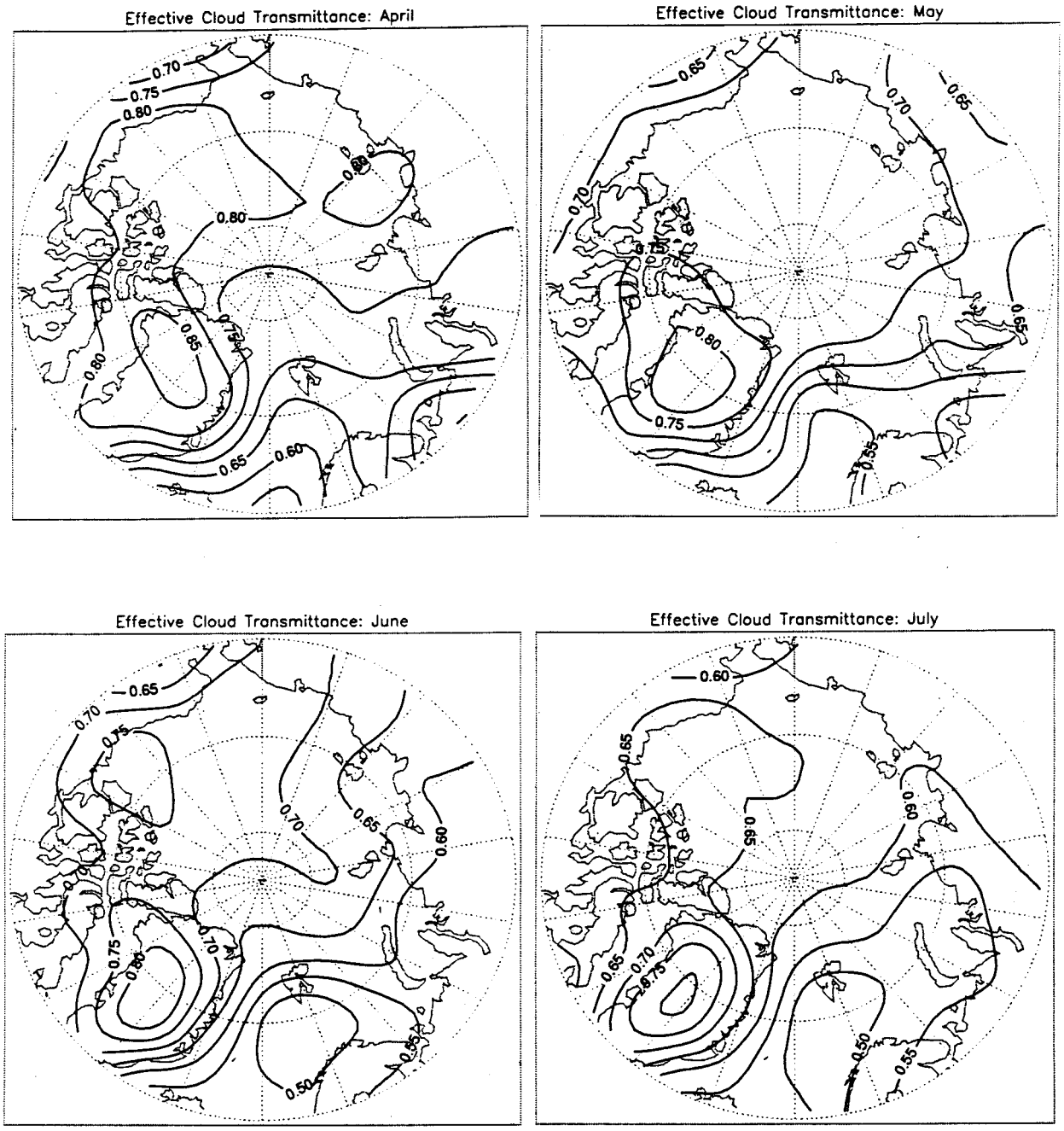


FIG. 4. Effective cloud transmittance for Apr–Sept.

by Schweiger and Key (1992), and the warm and cold season analyses of Clark et al. (1996).

### *b. Observed global radiation fluxes*

Our monthly gridded global radiation fields for March–October illustrate these basic controls (Fig. 3). Maps are displayed with a contour interval of 20 W $m^{-2}$. March, September, and October show a primarily zonal pattern, illustrating the dominant effects of the strong latitudinal decrease in $G_{clr}$ for these months. Comparatively large fluxes for these months are found over the southern part of the Greenland Ice Sheet, representing the tendency for the higher TOA flux at the lower latitudes to be locally enhanced by the elevation effect on path length. By contrast, April–August are instead dominated by a strong asymmetric pattern. Greenland shows a pronounced peak over its central portions from May through August, illustrating both the elevation effect on path length and the tendency for the

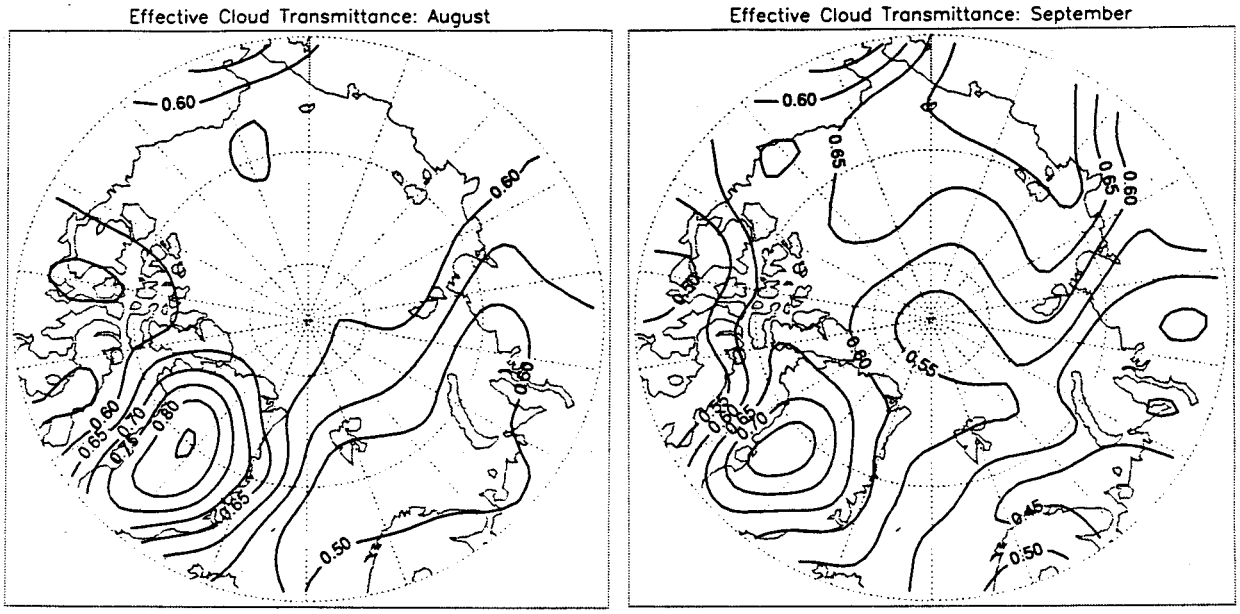


FIG. 4. (*Continued*)

high central portions of the ice sheet to be above the bulk of cloud cover. In turn, fluxes decrease sharply toward the Atlantic side, largely a function of increasing cloud amount.

There is also some tendency in summer months for a latitudinal increase in mean monthly fluxes, most apparent for June when $G_{clr}$ shows a marked increase with latitude, about 20 W m$^{-2}$ from 65°–90°N. Although cloud cover attenuates the flux, the higher central Arctic values in summer likely in part also manifest the offsetting effects of the high sea-ice surface albedo in promoting multiple scattering between the surface and clouds. For June, the month of maximum insolation, fluxes over the high-elevation Greenland ice sheet peak at more than 340 W m$^{-2}$, but with values in excess of 300 W m$^{-2}$ found over the Pacific side of central Arctic Ocean extending southward into the Beaufort Sea. June cloud cover is known to be relatively limited over the latter area. Fluxes of less than 200 W m$^{-2}$ characterize the Atlantic side in the Norwegian and Barents seas.

TABLE 1. Gridpoint correlations between monthly mean global radiation fields.

| | Obs. vs NCEP–NCAR | Obs. vs ISCCP-C2 | NCEP–NCAR vs ISCCP-C2 |
|---|---|---|---|
| Mar | 0.98 (0.55) | 0.97 (0.80) | 0.98 (0.45) |
| Apr | 0.89 (0.84) | 0.85 (0.54) | 0.92 (0.66) |
| May | 0.91 (0.88) | 0.84 (0.76) | 0.86 (0.79) |
| Jun | 0.83 (0.75) | 0.88 (0.84) | 0.93 (0.90) |
| Jul | 0.76 (0.72) | 0.80 (0.77) | 0.90 (0.88) |
| Aug | 0.69 (0.80) | 0.85 (0.89) | 0.84 (0.90) |
| Sept | 0.88 (0.75) | 0.87 (0.80) | 0.96 (0.87) |
| Oct | 0.94 (0.26) | 0.90 (0.79) | 0.97 (0.36) |

### *c. Effective cloud transmittance*

As described in section 4a, and illustrated in Figs. 2 and 3, the primary influences on spatio-temporal variations in surface global radiation are solar zenith angle/day length, path length, and clouds. To isolate the net effect of clouds, the first two effects can be removed by calculating an effective cloud transmittance $t$ for each grid cell:

$$t = G_{obs}/G_{clr}.$$

The quantity $t$ is primarily a cloud property because the effects of the atmosphere are removed through the use of the surface clear-sky global radiation rather than the TOA flux. It takes a value of one for clear sky (assuming that the modeled $G_{clr}$ is error free) and decreases toward zero with increasing cloud optical thickness and/or increasing cloud fraction. It is not a true cloud transmittance, which is the ratio of downwelling shortwave fluxes immediately below and above the cloud, because it includes the effects of multiple reflections between the surface and the cloud as well as the surface and the atmosphere, which are in turn related to surface albedo and because the cloud amount is unknown. The unknown cloud amount is related to the effective transmittance and the true cloud transmittance by

$$t = (1 - f) + ft_{cld},$$

where $f$ is the cloud fraction and $t_{cld}$ is the true cloud transmittance. We therefore use the term ''effective cloud transmittance'' to identify these shortcomings.

Fields of $t$ are shown in Fig. 4 for April–September. Following earlier discussion, other months are not dis-

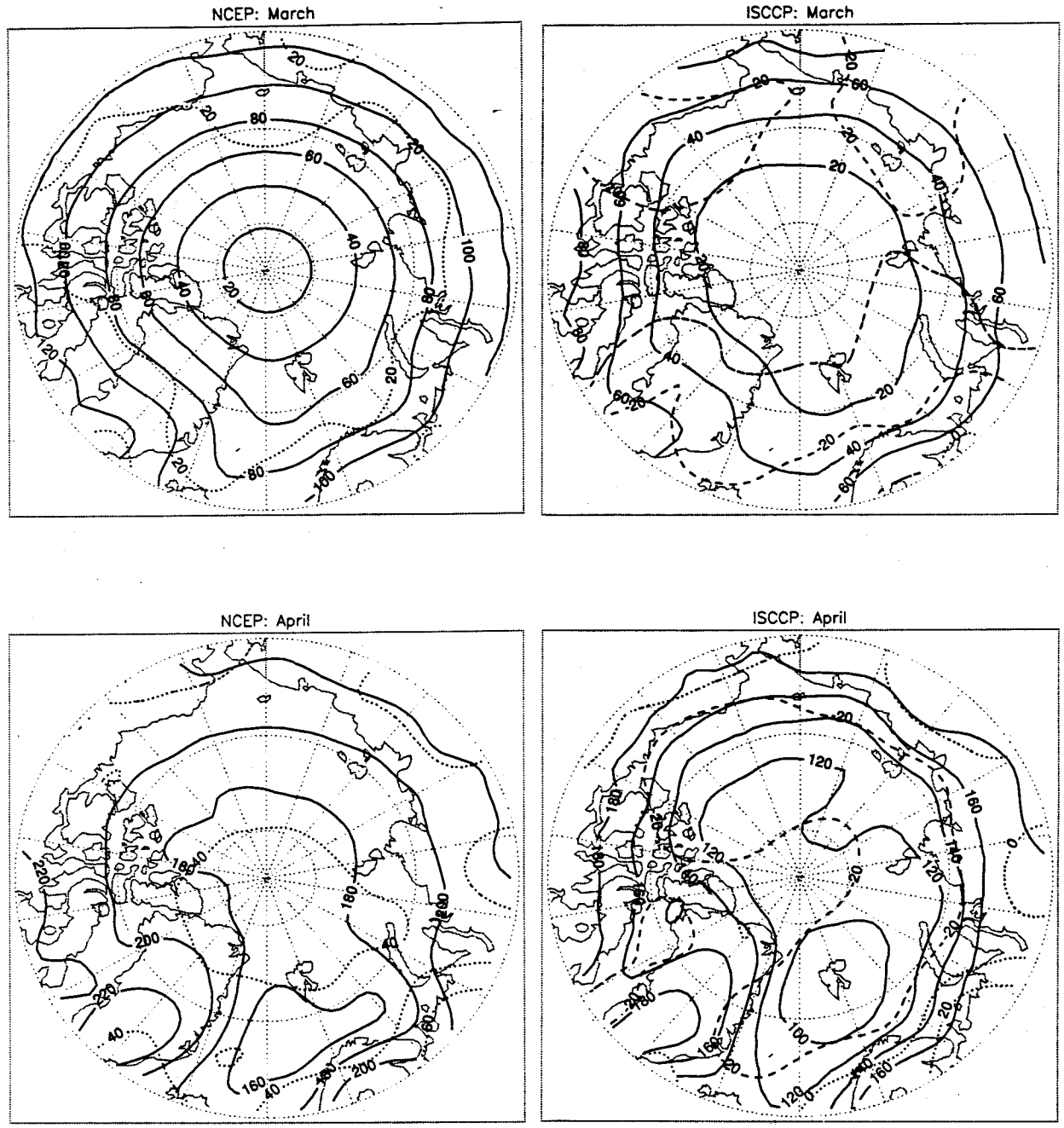


FIG. 5. Monthly average global radiation fluxes (Mar–Oct) from the NCEP–NCAR reanalysis and ISCCP-C2 product and departures from observed climatology (both in W $m^{-2}$). Contour lines for departures are dotted for positive values and dashed for negative values.

cussed as $t$ is strongly influenced by errors in measurement and estimation of clear-sky fluxes under extreme solar zenith angles. From April through August, the spatial patterns of $t$ are similar to the patterns of $G_{obs}$ in showing the highest values over Greenland (above 0.80), fairly high values over the ice-covered central Arctic Ocean with values falling toward the Atlantic side of the Arctic. This further demonstrates the dominance of cloud effects on the spatial distribution of $G_{obs}$ for these months rather than $G_{clr}$. As cloud cover during summer tends to be more spatially homogeneous, the summer pattern for $t$ also argues for a greater optical thickness of Atlantic side clouds. For the ice-covered central Arctic Ocean, $t$ ranges from 0.75 to 0.85 in April, falling to 0.60 to 0.65 in September. June shows a closed contour of relatively high values over the Beaufort Sea, where mean anticyclonic conditions tend to persist and cloud cover is suppressed. In contrast to April–August,

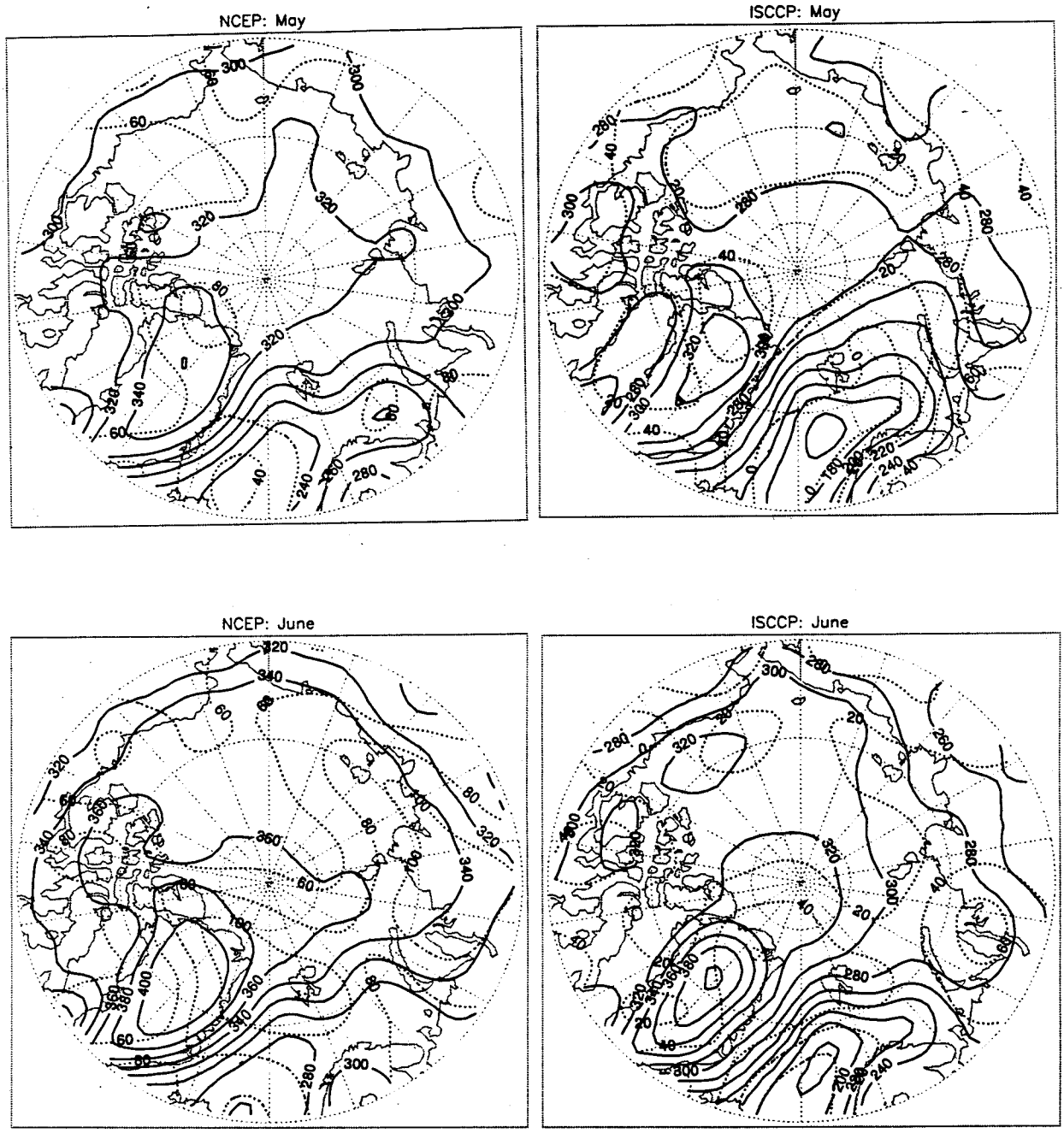


FIG. 5. (*Continued*)

September shows no marked relationship between $G_{obs}$ and $t$. This again demonstrates the effects of the strong latitudinal gradient in $G_{clr}$ for this month.

## 5. Comparisons with other climatologies

### *a. Surface-based climatologies*

Comparisons with earlier surface-based radiation climatologies are arguably not particularly meaningful. Due to the sparsity of data, particularly over the Arctic Ocean, most earlier studies have simply reported results for individual stations or as regional averages. At least three studies have attempted to provide spatial fields of global radiation (Marshunova and Chernigovskii 1971; Gavrilova 1963; Vowinkel and Orvig 1964), but these are not available in digital form and are based largely on estimated values rather than direct observations. Given our more extensive observational database, there is no reason to expect

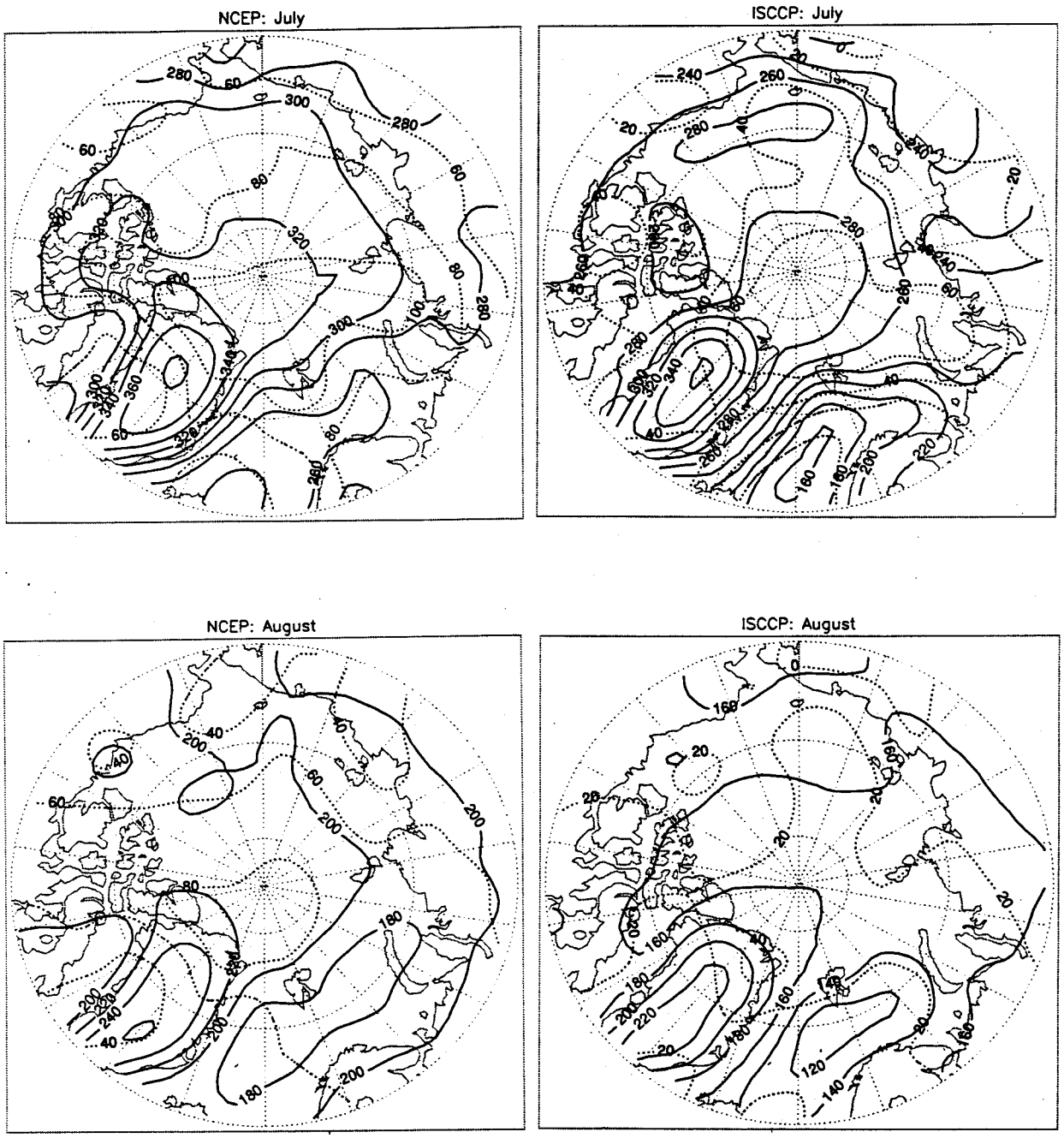


FIG. 5. (*Continued*)

quantitative agreement. Nevertheless, a few general comparisons are useful.

The monthly maps of Marshunova and Chernigovskii (1971) for February–October are based on measured values for 15 land stations as well as estimated values for 22 meteorological stations and 70 additional points over the Arctic Basin. Oddly, it does not appear that direct or calculated values from the NP drifting stations are used. While their Fig. 1 indicates points corresponding to T-3, it appears that calculated, rather than measured, values were used, despite available observations listed in their appendix III. No information is presented for the Greenland Ice Sheet.

Like our analysis, they depict a primarily zonal distribution of radiation for early spring and late autumn, with spring and summer displaying minimum values over the Atlantic side of the Arctic. However, they fail to show the relatively high values in the Beaufort Sea during June, presumably reflecting the lack of radiation or cloud observations in this region. Maximum values

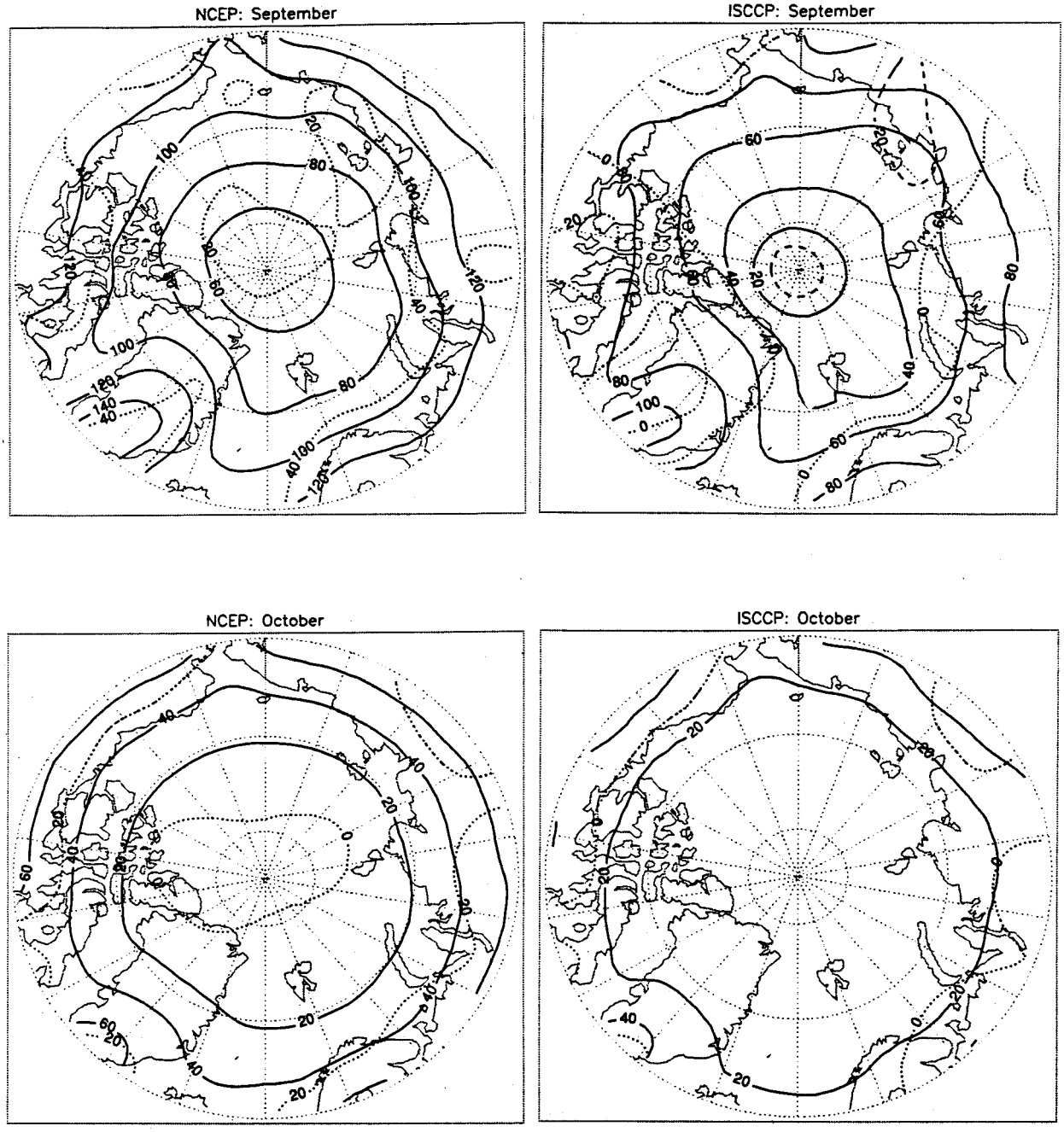


FIG. 5. (*Continued*)

north of Greenland are indicated. Vowinkel and Orvig (1964) provide maps for March and June, also based on calculated values but for fewer points. Not surprisingly, their March map effectively captures the zonal pattern of the flux seen in Fig. 3 when the latitudinal gradient of $G_{clr}$ is steep. However, their June map is very similar to that of Marshunova and Chernigovskii, also failing to capture the relative Beaufort Sea maximum. The same can be said of the maps of Gavrilova (1963), which are also based largely on estimated values but do include actual NP measurements. None of the NP stations at that time, however, provided Beaufort Sea coverage.

### *b. NCEP–NCAR and ISCCP-C2*

The joint National Centers for Environmental Prediction–National Center for Atmospheric Research (NCEP–NCAR) reanalysis project (Kalnay et al. 1996) is providing internally consistent gridded fields that will eventually span a 40-yr time period (1957–96). The

NCEP–NCAR fields are hoped to represent improvements over earlier numerical weather prediction products as a result of 1) the elimination of discontinuities through the use of a ''frozen'' state-of-the-art T62 model and data assimilation system, and 2) concerted efforts to use all available historical data in the assimilations with strict quality control. Along with temporally consistent analyzed atmospheric fields, a suite of modeled fields is provided, including all components of the surface radiation balance. Details of the NCEP–NCAR system are provided by Kalnay et al. (1996). As of this writing, 13 yr (1983–95) of the 6-h radiation fields were available.

Schweiger and Key (1994) used the ISCCP-C2 monthly cloud product to generate a gridded dataset of surface and TOA radiative fluxes and surface albedo over the Arctic Ocean for the period 1984–90. ISCCP-C2 (Rossow and Schiffer 1991) is a compilation of gridded monthly satellite-derived cloud statistics, surface reflectivity, atmospheric temperature, water vapor, and other variables. The data have a spatial resolution of about 280 km. The grids have constant 2.5° latitude increments and variable longitude increments, ranging from 2.5° at the equator to 120° at the pole. Radiative fluxes were computed for each ISCCP grid. For the computations, a background tropospheric aerosol amount was assumed; water vapor and ozone are part of the ISCCP data product. The procedure employed a two-stream radiative transfer model with 24 shortwave and 105 longwave spectral bands, optical property models for liquid clouds, and Arctic aerosols and mixed-surface albedo parameterizations. While we believe that the primary source of uncertainty in this flux dataset is uncertainty in the input data, we recognize that other methodologies might produce somewhat different surface radiative fluxes, for example, using daily or three-hourly input data (rather than our monthly values) and using a different radiative transfer model (cf. Rossow and Zhang 1995).

The NCEP–NCAR and ISCCP-C2 fields for March–October were interpolated to the EASE-grid using Cressman weights with a 500-km search radius. Grid-point correlations were then calculated between the observed and ISCCP-C2 fields, observed and NCEP–NCAR fields, and the ISCCP-C2 and NCEP–NCAR fields (Table 1). Correlations were computed using both the ''raw'' grid values and with grid values expressed as departures from $G_{clr}$ as calculated earlier (in parentheses), hence filtering out solar zenith angle/day length and path length effects. Results using the raw grid values argue that the ISCCP-C2 and NCEP–NCAR fields capture reasonably well the observed spatial patterns of global radiation; all correlations are above 0.80 (i.e., more than 60% of the spatial variance explained) except for July and August between the observed and NCEP–NCAR fields. However, these correlations in part reflect latitudinal dependencies common to all three datasets. Not surprisingly, removing these effects generally, but not always, results in lower correlations. The ''adjusted'' correlations between the observed and NCEP–NCAR and observed and ISCCP-C2 fields range from about 0.70–0.85 from May through August. The adjusted observed versus NCEP–NCAR correlations drop sharply in March and October, with ISCCP-C2 performing poorly in April; this accounts for the low correlations for these three months between the NCEP–NCAR and ISCCP-C2 fields, which are otherwise rather high.

Figure 5 shows the March–October NCEP–NCAR and ISCCP-C2 fields averaged over their respective periods of the record along with corresponding departures from $G_{obs}$. It is evident that both radiation products capture the major features of maximum fluxes over Greenland, the seasonal north–south migration of this feature, and strong zonal flux patterns for March, September, and October, with other months showing an asymmetric pattern with an Atlantic side minimum. However, neither field effectively captures the relative maximum from near the pole extending into the Beaufort Sea observed for June, although ISCCP-C2 does give some indication of this feature. We find that for all months, the adjusted correlations tend to be anchored by the high values in all three fields over Greenland. Correlations drop by typically 0.10 when Greenland grid points are removed from the calculations.

The more basic problem is in the flux magnitudes, which are too high, especially for the NCEP–NCAR fields. The error contours in Fig. 5 reveal the NCEP–NCAR fluxes as high everywhere for every month. Errors for June, the month of maximum insolation, range from 60 to 80 W $m^{-2}$ over most of the Arctic Ocean, growing over Siberia and toward the Atlantic side of the Arctic, although in fairness we stress that our fluxes for the latter region largely represent estimated values. ISCCP-C2 departures are consistently smaller, typically 20–40 W $m^{-2}$ over the Arctic Ocean for most months. On the other hand, ISCCP-C2 appears to underestimate fluxes by about 20 W $m^{-2}$ during spring and autumn and notably March and April.

These errors are fundamentally related to cloud cover. From comparisons with available climatologies, ISCCP-C2 appears to underestimate cloud fractions by typically 5%–35%, with the errors greatest during summer (Schweiger and Key 1992). Not surprisingly, comparisons with summaries for the region north of 75°N from the Marshunova (1961) climatology indicate that the downwelling longwave fluxes are in general too low, although the global radiation fluxes are in good agreement (Schweiger and Key 1994). While not entirely resolved, this appears to result from the negative bias in cloud fractions to be offset by optical thickness values that are too high. The comparisons in Fig. 5 suggest that this balancing effect on global radiation fluxes is nevertheless incomplete.

Our analysis indicates that the NCEP–NCAR model correctly depicts the basic observed pattern of higher

cloud fractions over the Atlantic side of the Arctic, in accord with the modeled Atlantic-side radiation minimum. However, as averaged for the region north of 70°N, the NCEP–NCAR cloud fraction has an annual average of only about 40% and furthermore exhibits only a weak seasonal cycle, ranging by about 10% from a winter–spring minimum to a summer–autumn maximum. This compares to annual mean values from different available surface climatologies of typically 70%–80% with a summer maximum. An oversight in archiving the NCEP–NCAR output precludes assessments of low, middle, and high cloud amounts. However, some estimate of the cloud problem can be obtained by estimating the effective cloud transmittance ($t$) based on the NCEP–NCAR global radiation fluxes and $G_{clr}$. Our estimate of $t$ for the central Arctic Ocean for June is 0.65–0.75 (Fig. 4) compared to the modeled values, which are 0.15–0.20 higher (not shown). Similar errors characterize other months. By comparison, $t$ calculated using the ISCCP-C2 global radiation fluxes tends to be within 0.05–0.10 of our values.

## 6. Summary and conclusions

Arctic Ocean measurements from the Russian North Pole series of drifting stations, records from the United States drifting stations T-3 and Arlis II, existing archives for land stations, and, where necessary, around coastal Greenland and the northern North Atlantic, estimated values are used to compile a new gridded monthly climatology of global radiation for the region north of 65°N.

The distribution of global radiation is primarily zonal for March, September, and October, when latitudinal gradients in the clear-sky flux are pronounced. Other months are characterized by a strong asymmetric pattern with peak fluxes over central Greenland and low values over the North Atlantic. The Greenland peak represents the effect of elevation with the Atlantic-side minimum resulting from more extensive cloud cover. For June, the month of maximum insolation, fluxes over the Atlantic side of the Arctic are locally less than 200 W $m^{-2}$, compared to more than 300 W $m^{-2}$ for the Pacific side of central Arctic Ocean extending into the Beaufort Sea and more than 340 W $m^{-2}$ over Greenland. Effective cloud transmittance, estimated for April–September, shows patterns similar to that for global radiation for all months except September, further illustrating the role of cloud cover in controlling the spatial distribution of the global radiation flux.

The spatial patterns of monthly fluxes as depicted in the NCEP–NCAR reanalysis and fluxes computed using the ISCCP-C2 cloud product correlate reasonably highly (0.70–0.85) with our climatology during most months. However, NCEP–NCAR reanalysis fluxes are much too high for all months, which fundamentally relates to large underestimates in cloud fraction or optical thickness, although the general spatial patterns of cloud cover appear reasonable. Fluxes based on the ISCCP-C2 data are also generally too high, but with smaller departures than for the NCEP–NCAR reanalysis. A preliminary examination of the reprocessed ISCCP monthly cloud product (D2) for 1990 indicates that cloud amounts in the Arctic are somewhat higher, and optical depths are lower than in the C2 data.

We plan to improve upon our global radiation climatology through the acquisition of updates to the GEBA and PARCA archives and Beaufort Sea data to be collected during the upcoming SHEBA field experiment. Efforts are also under way to compile a similar climatology of net radiation. Work is also underway to process the new ISCCP-D product and to validate these fields against our observed climatologies.

*Acknowledgments.* This study was supported by NSF Grants OPP-9321547, OPP-9504201, and OPP-9614297. Additional support was provided by NASA Grant NAGW-2407. We thank the anonymous reviewers for their constructive comments.

REFERENCES

Armstrong, R. L., and M. J. Brodzik, 1995: An earth-gridded SSM/I data set for cryospheric studies and global change monitoring. *Adv. Space Res.*, **16** (10), 155–163.

Clark, M. P., M. C. Serreze, and R. G. Barry, 1996: Characteristics of Arctic Ocean climate based on COADS data, 1980–93. *Geophys. Res. Lett.*, **23** (15), 1953–1956.

Cressman, G. P., 1959: An operational objective analysis system. *Mon. Wea. Rev.*, **87,** 367–374.

Curry, J. A., W. B. Rossow, D. Randall, and J. L. Schramm, 1996: Overview of Arctic cloud and radiative characteristics. *J. Climate*, **9,** 1731–1764.

Fletcher, J. O., 1966: The Arctic heat budget and atmospheric circulation. *Proc. Symp. Arctic Heat Budget and Atmospheric Circulation,* Lake Arrowhead, CA, Rand Corp., 23–43.

Gavrilova, M. K., 1963: *Radiatsionnyi Klimat Arktiki (Radiation Climate of the Arctic).* Gidrometeorologicheskoe Izdatel'stvo, 178 pp.

Hahn, C. J., S. G. Warren, and J. London, 1995: The effect of moonlight on observations of cloud cover at night and application to cloud climatology. *J. Climate,* **8,** 1429–1446.

Herman, G. F., 1977: Solar radiation in summer Arctic stratus clouds. *J. Atmos. Sci.,* **34,** 1425–1432.

——, and J. A. Curry, 1984: Observational and theoretical studies of solar radiation in Arctic stratus clouds. *J. Climate Appl. Meteor.*, **23,** 5–24.

Huschke, R. E., 1969: Arctic cloud statistics from air calibrated surface weather observations. Rand Corp. Memo. RM-6173-PR, Santa Monica, CA, 79 pp.

IPCC, 1990: *Climate Change: The IPCC Scientific Assessment.* Cambridge University Press, 365 pp.

Jacobs, J. J., R. G. Barry, R. S. Bradley, and R. L. Weaver, 1974: Studies of climate and sea ice conditions in Eastern Baffin Island, 1971–1973. Occasional Paper No. 9, Institute for Arctic and Alpine Research, University of Colorado, Boulder, CO, 78 pp.

Kalnay, E., and Coauthors, 1996: The NCEP/NCAR 40-yr reanalysis project. *Bull. Amer. Meteor. Soc.*, **77,** 437–471.

Key, J., 1997: Streamer user's guide. Dept. of Geography, Boston University, Tech. Rep. 96-01, 85 pp.

——, E. Amano, and J. Collins, 1997: FluxNet user's guide. Tech. Rep. 96-03, 22 pp.

——, R. S. Silcox, and R. S. Stone, 1996: Evaluation of surface

radiative flux parameterizations for use in sea ice models. *J. Geophys. Res.,* **101**(C2), 3839–3849.

Marshunova, M. S., 1961: *Principle Regularities of the Radiation Balance of the Underlying Surface and of the Atmosphere in the Arctic* (in Russian). Tr. Arkt. Antarkt. Nauchno-Issled. Inst., 52 pp.

——, and N. T. Chernigovskii, 1966: Numerical characteristics of the radiation regime in the Soviet Arctic. *Proc. Symp. Arctic Heat Budget and Atmospheric Circulation,* Lake Arrowhead, CA, Rand Corp., 279–297.

——, and ——, 1971: *Radiatsionnyi Rezhim Zarubeznhoi Arktiki (Radiation Regime of the Foreign Arctic).* Gidrometeorologicheskoe Izdatel'stvo, 182 pp.

——, and A. A. Mishin, 1994: Handbook of the radiation regime of the Arctic basin (results from the drift stations). Tech. Rep. APL-UW TR 9413, Applied Physics Laboratory, University of Washington, Seattle, WA, 52 pp. plus appendices.

Muller, F., and Coauthors, 1976: Report on North Water Project Activities, 1 October 1975 to 30 September 1976. Progress Rep. IV, ETH, Zurich, Switzerland, 54 pp.

Ohmura, A., 1981: *Climate and Energy Balance of Arctic Tundra.* Vol. 3, *Zürcher Geographische Schriften,* ETH Geographisches Institut, 447 pp.

——, and H. Gilgen, 1991: Global Energy Balance Archive GEBA. Report 2: The GEBA Database, Interactive Applications, Retrieving Data. Internal Rep., Department of Geography, ETH, Zurich, 66 pp.

Pautzke, C. G., and G. F. Hornof, 1978: Radiation program during AIDJEX: A data report. AIDJEX Bulletin No. 39, Arctic Ice Dynamics Joint Experiment, Division of Marine Resources, University of Washington, Seattle, 165–185.

Raschke, E., P. Bauer, and H. J. Lutz, 1992: Remote sensing in the polar regions. *Int. J. Remote Sensing,* **1,** 23–35.

Rossow, W. B., and R. A. Schiffer, 1991: ISCCP cloud data products. *Bull. Amer. Meteor. Soc.,* **72,** 2–20.

——, and Y.-C. Zhang, 1995: Calculation of surface and top-of-atmosphere radiative fluxes from physical quantities based on ISCCP datasets, part II: Validation and first results. *J. Geophys. Res.,* **100** (D1), 1167–1197.

Roulet, R. R., 1969: Radiation regime of Arctic drifting station Arlis II, January 1964–May 1965. Department of Atmospheric Sciences, University of Washington, Scientific Rep., Office of Naval Research Contract N00014-67-A-0103-0007, NR 307–252, 58 pp.

Schmetz, J., 1989: Towards a surface radiation climatology. Retrieval of downward irradiances from satellites. *Atmos. Res.,* **23,** 287–321.

Schweiger, A. J., and J. R. Key, 1992: Arctic cloudiness: Comparison of ISCCP-C2 and Nimbus-7 satellite-derived cloud products with a surface-based cloud climatology. *J. Climate,* **5,** 1514–1527.

——, and ——, 1994: Arctic Ocean radiative fluxes and cloud forcing estimated from the ISCCP C2 cloud dataset, 1983–1990. *J. Appl. Meteor.,* **33,** 948–963.

——, M. C. Serreze, and J. R. Key, 1993: Arctic sea ice albedo: A comparison of two satellite-derived data sets. *Geophys. Res. Lett.,* **20** (1), 41–44.

Serreze, M. C., and M. C. Rehder, 1990: June cloud cover over the Arctic Ocean. *Geophys. Res. Lett.,* **17,** 2397–2400.

——, J. E. Box, R. G. Barry, and J. E. Walsh, 1993: Characteristics of Arctic synoptic activity, 1952–1989. *Meteorol. Atmos. Phys.,* **51,** 147–164.

——, ——, R. G. Barry, J. D. Kahl, and N. A. Zaitseva, 1995: The distribution and transport of atmospheric water vapour over the Arctic. *Int. J. Climatol.,* **15,** 709–727.

Shine, K. P., 1984: Parameterization of shortwave flux over high albedo surfaces as a function of cloud thickness and surface albedo. *Quart. J. Roy. Meteor. Soc.,* **110,** 747–764.

——, A. Henderson-Sellers, and R. G. Barry, 1984: Albedo-climate feedback: The importance of cloud and cryosphere variability. *New Perspectives in Climate Modeling, Development in Atmospheric Sciences,* A. Berger and C. Nicolis, Eds., Elsevier, 135–155.

Smetannikovoi, A. V., 1983: *Radiation Regime of the of the Greenland and Norwegian Seas* (in Russian). Gidrometeoizdat, 64 pp.

Stamnes, K., S. C. Tsay, W. Wiscombe, and K. Jayaweera, 1988: Numerically stable algorithm for discrete-ordinate method radiative transfer in multiple scattering and emitting layered media. *Appl. Opt.,* **27,** 2502–2509.

Toon, O. B., C. P. McKay, and T. P. Ackerman, 1989: Rapid calculation of radiative heating rates and photodissociation rates in inhomogeneous multiple scattering atmospheres. *J. Geophys. Res.,* **94** (D13), 16 287–16 301.

Vowinckel, E., and S. Orvig, 1962: Insolation and absorbed solar radiation at the ground in the Arctic. Publications in Meteorology, No. 53, McGill University, Montreal, Quebec, Canada, 32 pp.

——, and ——, 1963: Long wave radiation and total radiation balance at the surface in the Arctic. Publications in Meteorology, No. 62, McGill University, Montreal, Quebec, Canada, 33 pp.

——, and ——, 1964: Energy balance of the Arctic. I. Incoming and absorbed solar radiation at the ground in the Arctic. *Arch. Meteor. Geophys. Bioklimatol.,* **13** (3), 352–377.

Warren, S. G., C. J. Hahn, J. London, R. M. Chervin, and R. Jenne, 1986: Global distribution of total cloud cover and cloud type amounts over land. NCAR Tech. Note TN-273+STR, Boulder, CO, 29 pp.

——, ——, ——, ——, and ——, 1988: Global distribution of total cloud cover and cloud type amounts over the ocean. NCAR Tech. Note TN-317+STR, Boulder, CO, 41 pp.

Weller, G., and B. Holmgren, 1974: Summer global radiation and albedo—Data for three stations in the Arctic basin, Ice Island T-3, Barrow, Prudhoe Bay, 1971–1973. Tech. Rep. No. 2, December 1974, Geophysical Institute, University of Alaska, Fairbanks, 31 pp.

Wendler, G. W., F. D. Eaton, and T. Ohtake, 1981: Multiple reflection effects on irradience in the presence of Arctic stratus clouds. *J. Geophys. Res.,* **86** (C3), 2049–2057.

WMO, 1992: Report on the workshop on polar radiation fluxes and sea-ice modelling. World Climate Research Programme, WMO/TD No. 442, 20 pp.